Development of a Snow Erosion Test Capability for the Hyperballistic Range

E. Eugene Callens Jr.,* James R. Blanks,† and Dwayne B. Carver‡
ARO, Inc., Arnold Air Force Station, Tenn.

A unique snow erosion test capability has been developed for the AEDC-VKF 1000-ft Hyperballistic Range G. Erosion tests now can be conducted at encounter velocities up to 19,000 fps, freestream pressures from a few millimeters of mercury to 1 atm, and snowfield concentrations that correspond to those occurring in the natural environment (down to 0.05 gm/m^3). The snowfield can be extended over several hundred feet, allowing the erosion process to be investigated with or without ablation coupling.

Nomenclature

A_n = reference nose-tip frontal area, $\pi(0.707\ r_n)^2$
A_p = nose-tip semiprofile eroded area
A_r = snowfield reference area centered on the model penetration point
c_s = snowfield concentration, $m_s/A_n\ell_s$
$\bar{d}$ = diameter of the "mass mean" snowflake
$\bar{d}_i$ = diameter of the mass mean snowflake in the ith size range
G = mass removal ratio (m_n/m_s)
$k(\bar{d}_i)$ = snowfield correlation parameter, function of flake size, units of density
ℓ_s = length of the encountered snowfield
m_j = measured mass in the jth correlation experiment
m_n = mass of material removed from the nose tip within a right circular cylinder of base radius 0.707 r_n whose axis coincides with the nose-tip axis (reference volume)
m_r = apparent mass removed from the nose tip within the reference volume as determined from in-flight laser photographs (uncorrected for hidden surface contour bias)
m_s = mass of snow impacted by the reference nose tip frontal area (A_n)
m_{s_r} = mass of snow within the snowfield reference area (A_r)
N_i = number of snowflakes in the ith size range
$\bar{N}$ = number of mass mean snowflakes within the snowfield reference area (A_r)
$\bar{N}_i$ = number of mass mean snowflakes impacted by the reference nose tip frontal area, defined by Eq. (8)
n = number of instrumented encountered snowfields
r = radius of nose-tip frontal area, 0.707 r_n
r_n = model nose-tip radius
V_i = volume of all flakes in the ith size range
$V_{i,j}$ = volume of all flakes in the ith size range in the jth snowfield correlation experiment
V_r = apparent volume of material removed from the nose tip within the reference volume
$\bar{y}$ = centroid of the area (A_p) about the model axis
θ_p = angle between the snowfield reference plane and the range centerline
ξ = ratio of the total number of encountered snowfields to the number of measured encountered snowfields
ρ_n = density of the model nose-tip material
ΣA_i = area of all snowflakes in the ith size range
σ = standard deviation

Presented at the AIAA 9th Aerodynamic Testing Conference, Arlington, Texas, June 7-9, 1976 (in bound volume of Conference papers, no preprint number); submitted June 24, 1976; revision received Oct. 28, 1976.

Index categories: Research Facilities and Instrumentation; Hypervelocity Impact; Material Ablation.

*Research Engineer, Aeroballistics Branch, von Karman Gas Dynamics Facility (VKF). Member AIAA.

†Project Engineer, Aeroballistics Branch, VKF.

‡Project Engineer, Aerodynamics Projects Branch, VKF.

Introduction

ONE of the potential hazards of a re-entry vehicle (RV) is hypervelocity encounter with liquid or solid particles that occur in the natural environment. In order to understand and evaluate, at a reasonable cost, the effect of hydrometeor particles on RV's in conjunction with the high aerodynamic heating loads associated with re-entry, it is necessary to conduct ground tests which simulate re-entry conditions.

The facility which has proven to be most effective for this type of testing is the hyperballistic range with its capability of duplicating simultaneously encounter velocity, stagnation enthalpy, and stagnation pressure corresponding to a point in the re-entry trajectory.[1] Additionally, the range permits detailed erosive environment characterization, as the erosive fields are generated under static conditions.

A particular erosive environment of interest is snow, because of the existence of snow crystals in very high-altitude clouds and the resulting relatively high probability of encountering these crystals during re-entry in cloudy weather. In order to acquire meaningful data under realistic test conditions, it is required to generate snow crystals having a crystalline structure similar to those occurring in the atmosphere.

Snowfield Generation

The mechanism of formation for natural ice crystals is the diffusion of water vapor to the growing crystal surfaces. That is, the solid crystal is formed directly from the water molecules by sublimation with no bulk liquid phase (although there may be a thin liquid layer at the surface of the crystal). The ice crystals grow from nuclei in an ice-supersaturated atmosphere and may exist as individual units of simple geometrical shape, or under suitable conditions, may grow into complex branched forms. Several of these snow crystals may cluster to form a snowflake.

A marked difference between these crystals and other ice forms such as sleet or hail is illustrated by the particle bulk density, defined as the mass of the particle divided by the volume of the smallest sphere that will completely enclose the particle without altering its shape. A near spherical 1-mm-diam ice particle has a bulk density of approximately 0.9 gm/cc, whereas a dendritic snow crystal with a maximum diameter of 1 mm has a bulk density of the order of 0.02 gm/cc, a factor of 45 difference. More detailed information

on the mechanisms of formation and characteristics of atmospheric hydrometeors is presented in Refs. 2 through 7.

In order to generate snowflakes having an appropriate bulk density and crystalline type, a method of growing crystals on solid surfaces was developed in which the formation process is the same as for natural snow, namely, the diffusion of water vapor to the growing surface. This technique is based on the fact that both snow and frost crystals have the same mechanism of formation and have similar crystalline characteristics for the same thermodynamic conditions. Nakaya[2] demonstrated the correspondence of crystalline frost to various types of snow crystals including the dendritic type. The primary difference between snow and frost is that a snow crystal grows from a nucleus in the free atmosphere, whereas the frost crystal grows from a solid surface. The most obvious visual effect of this difference in nuclei is in the dendritic forms where snow grows as symmetrical six-branched crystals and frost grows as single-branched crystals.

However, a natural snowflake consists of a number of these individual crystals that are clustered together in some random orientation. Likewise, the generated snowflakes formed when frost crystals are dislodged from their growing surface are clusters of randomly oriented single-branched crystals. These flakes are similar in structure and size to those occurring in the atmosphere.

To apply this concept to the range environment, a piece of hardwaer referred to as a "snowfield generator" was developed. It is simply a copper plate with a copper tube bonded to it, through which a coolant flows. The plate temperature is measured by a thermocouple attached to the plate and regulated by a temperature controller which operates a flow control valve in the coolant circuit.

These snowfield generators are mounted typically 2 ft above the centerline at selected intervals along the range axis. The plates are vertical, but oriented in the horizontal plane at 45° to the longitudinal axis of the range to accommodate sidemounted cameras which photograph the falling snow. The snowflakes are dislodged from the copper plate by a mechanical shock device (solenoid plunger) at the desired time and produce a free-falling erosion field which can be varied in field length and concentration.

The snow erosion test capability described herein was developed for the AEDC-VKF 1000-ft Hyperballistic Range G.[8] A schematic of a typical snowfield generator installation is shown in Fig. 1. This particular range configuration, with the snowfields located in the downrange half of Range G, provides the capability for aerodynamically preheating the model prior to encounter with the erosion field. The range pressure can be staged by means of a fast-opening valve located 300 ft from range entrance.

The technique employed for generating a snowfield during a shot is as follows:

1) Liquid nitrogen is circulated through the generator tubes to maintain subfreezing temperature, typically from −50 to −90°F.

2) Crystals grow on the plates by the diffusion of water vapor to the growing surfaces.

3) The "loaded" plates are impacted at a synchronized time in the launch cycle.

4) The crystals break off, forming clusters which are structurally similar to natural snowflakes.

5) The resulting snowfield is penetrated by the model.

Instrumentation

The mass of snow impacted by the nose tip is evaluated from conventional front-lighted photographs of the snowfield taken a few milliseconds prior to model penetration. The plates of the snowfield generators are mounted at 45° to the range centerline to permit each camera to view the falling snow normal to the plane of the plate (Fig. 1). The cameras utilize 1-msec shutters, and the snowfields are illuminated by strobe lights of 1-μsec duration.

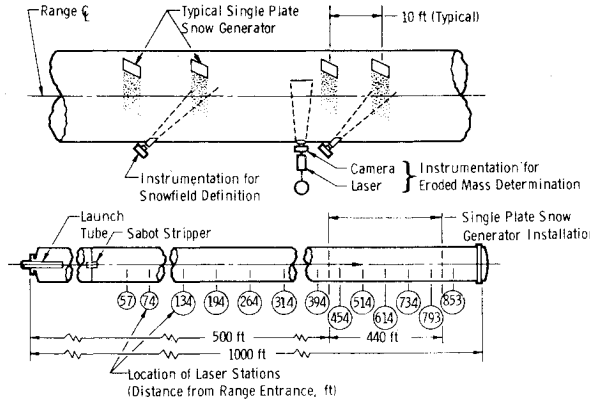

Fig. 1 Typical snowfield generator installation in AEDC Range G.

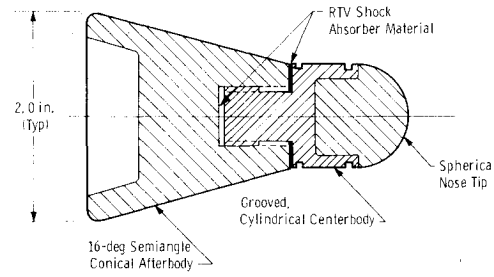

Fig. 2 Typical snow erosion model.

The mass of material removed from the nose tip is evaluated from front-lighted laser photographs of the in-flight model. The laser's short time duration, approximately 20 nsec, effectively "stops" the model motion at speeds up to 20,000 fps, and the high light intensity, approximately 75 MW of peak power, provides adequate film exposure. Also, the monochromaticity of the laser light allows filtering of unwanted light so that accurate measurements can be made from a laser photograph even under conditions of ablation, self-luminosity, and high density gradients.[9-13] With this system, the surface contour of the eroded nose tip generally can be measured to ±1.5 mils.

Several additional instrumentation systems are used in snow erosion testing. Range pressure, temperature, dew point, and the generator plate temperature are measured. The model trajectory is determined accurately from orthogonal shadowgrams taken at nominal 10- or 20-ft intervals. A single focused shadowgram can be taken 81 ft from the range entrance to visualize flowfield details. Several X-ray stations can be operated in the blast tank, uprange, and downrange of the snowfield to monitor model-sabot separation and supplement the laser coverage. Photo-optical pyrometric systems can be used to monitor surface temperature at 109, 211, 329, 395, 593, 734, and 853 ft from the range entrance. A sequence of photographs can be taken during snowfield encounter using a Beckman and Whitley high-speed framing camera. These instrumentation systems are described in more detail in Refs. 14 through 18.

Test Procedure

The basic test technique is to launch the model through the falling snow at a specified range pressure and model velocity. The crystal growth process is synchronized with the launch cycle. Snowfield concentration is controlled by regulating crystal growth time and filtering the falling snowflakes through perforated plates. Since the falling snow stratifies with larger flakes near the head of the fall and smaller ones near the tail, the impacted flake size can be controlled within the limits of model dispersion by appropriate timing of model arrival.

A typical snow erosion model consists of a hemispherical nose cap, followed by a cylindrical centerbody, and a 16° conical afterbody as shown in Fig. 2. The centerbody and nose cap are free to move parallel to the longitudinal axis of the model, the motion being damped by a room-temperature-vulcanized (RTV) shock absorber material. This technique for shock mounting the nose tip reduces stresses during launch and permits relatively fragile nose tip materials to be launched at velocities up to 19,000 fps. The grooves in the centerbody provide a scale factor and reference surfaces for measurement of in-flight nose-tip dimensions.

Data Analysis

The primary parameter of interest in erosion testing is the mass removal ratio which is the ratio of mass of material removed from a test specimen to the mass of erosive material impacted. In order to be able to specify the mass of material impacted it is required to characterize accurately the snowfield at the instant of model penetration. This is a difficult task for snow, as each snowflake is a highly porous, irregularly shaped collection of individual dendritic crystals.

Snowfield Calibration

Calibration experiments were designed to establish the relationship between snow mass and two-dimensional image data such as number and projected area of the flakes. These experiments were performed in the range under simulated test conditions. Variables controlled or monitored during the experiments were ambient pressure, ambient temperature, generator plate temperature, dew point, growth time, fall time, and number and spacing of snowflake filters.

In a typical experiment, the procedure is as follows:

1) Dendritic crystals are grown on a single plate under simulated test conditions.

2) At the appropriate time, the crystals are dislodged by impacting a solenoid plunger against the plate.

3) The resulting snowfall, approximately 3 ft in length when centered about the range axis, is photographed.

4) The snow is caught on a sheet of lightweight plastic film of known mass.

5) The plastic film is folded immediately and sealed to prevent mass loss because of evaporation.

6) The film plus snow is weighed on balances accurate to a tenth of a milligram and the film weight subtracted to obtain the snow mass.

The photograph of the snowfall is subsequently analyzed on a Quantimet Image Analyzing Computer which automatically records the number and total area of the snowflakes in each of 22 flake size ranges. These data then are analyzed as follows:

1) An average flake dimension is determined for each size range

$$\bar{d}_i = \left(\frac{\Sigma A_i}{N_i}\right)^{1/2} \tag{1}$$

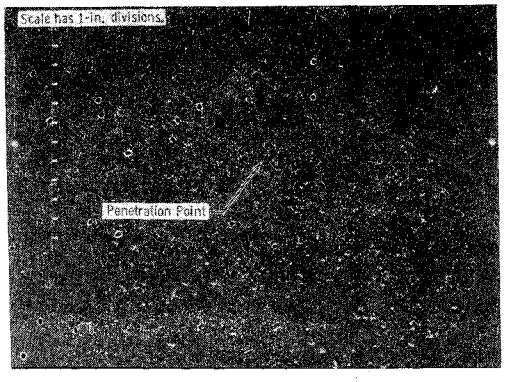

Fig. 3 Typical snowfield (approximately 7 msec before model arrival).

2) The volume of all the flakes in each size range i is determined as

$$V_i = N_i \bar{d}_i^3 \tag{2}$$

3) A set of equations is written based on the assumption that the density of the snowflakes is a function of flake size and the measured mass is the sum of the contributions from each of the 22 size ranges. Each equation represents a separate experiment as defined previously.

$$\begin{aligned}
&V_{1,1}k(\bar{d}_1) + V_{2,1}k(\bar{d}_2) + V_{3,1}k(\bar{d}_3) + \ldots + V_{22,1}k(\bar{d}_{22}) = m_1 \\
&V_{1,2}k(\bar{d}_1) + V_{2,2}k(\bar{d}_2) + V_{3,2}k(\bar{d}_3) + \ldots + V_{22,2}k(\bar{d}_{22}) = m_2 \\
&\quad\cdots\cdots\cdots\cdots\cdots \\
&V_{1,j}k(\bar{d}_1) + V_{2,j}k(\bar{d}_2) + V_{3,j}k(\bar{d}_3) + \ldots + V_{22,j}k(\bar{d}_{22}) = m_j
\end{aligned} \tag{3}$$

4) These equations are solved by a regression technique to obtain $k(\bar{d}_i)$.

Snowfield Characterization

During an actual range shot, high-resolution strobe-lighted photographs of the falling snow are taken a few milliseconds prior to model arrival. A typical photograph is shown in Fig. 3. The scale and ball in the picture provide a scale factor and a known reference location, respectively.

The points where the model penetrated the snowfield are located using trajectory data obtained from the orthogonal shadowgrams. Then, the snowflake area distribution in a "snowfield reference area" centered about the model penetration point is determined using the Quantimet Image Analyzing Computer. The mass of snow in the reference area is calculated by applying the previously determined correlation parameter $k(\bar{d}_i)$ to the Quantimet output data

$$m_{s_r} = \sum_{i=1}^{22} [k(\bar{d}_i)\, V_i] \tag{4}$$

The mass of snow impacted by the appropriate nose-tip reference frontal area A_n is

$$m_s = m_{s_r}(A_n/A_r)\csc\theta_p \tag{5}$$

Other statistical quantities of interest are computed from the basic area distribution. The mass mean flake dimension $\bar{d}$ within the reference area is given by

$$\bar{d} = \frac{\sum_{i=1}^{22} [k(\bar{d}_i)\, V_i d_i]}{\sum_{i=1}^{22} [k(\bar{d}_i)\, V_i]} \tag{6}$$

where

$$\sum_{i=1}^{22} [k(\bar{d}_i)\, V_i]$$

is the total flake mass within A_r. The number of these mean mass flakes within A_r is

$$\bar{N} = \frac{\sum_{i=1}^{22} [k(\bar{d}_i)\, V_i]}{k(\bar{d})\,\bar{d}^3} \tag{7}$$

and the number of mean mass snowflakes impacted by the nose tip is given by

$$\bar{N}_I = \bar{N}(A_n/A_r)\csc\theta_p \tag{8}$$

The total mass of snow impacted is the sum of the masses encountered at each snowfield. In practice, it is found to be satisfactory to instrument only a portion (e.g., 20 of 40) of the snowfields and statistically infer the unmeasured impacted masses. The expression for mass impacted at any given location is

$$m_s = \xi \frac{A_n}{A_r}\csc\theta_p \sum_{j=1}^{n}\left\{\sum_{i=1}^{22}[k(\bar{d}_i)V_i]\right\}_j \tag{9}$$

The snowfield concentration is calculated as

$$c_s = (m_s/A_n\ell_s) \tag{10}$$

Eroded Mass Determination

The mass of nose material removed is evaluated from in-flight laser photographs taken before, during, and after model encounter with the snowfields. In Fig. 4 a typical sequence of these photographs is presented. In the last photograph, the substrate stepcap of the test nose tip has been exposed. The model, which rolls at typically three turns per 1000 ft, presents a different profile at each laser station to an observer at a fixed angular position. In addition, there are several cameras at each laser station at different angular locations which frequently produce more than one photograph in sufficiently good focus to be of use. It is from these profiles that a measurement of the mass of material removed from the nose tip is made.

The volume associated with the mass removed is taken to be the region between the pre- and post-erosion profiles contained within the nose tip reference frontal area A_n (Fig. 5). The eroded mass is then obtained as follows:

1) An area A_p bounded by the model axis, the pre- and post erosion nose tip semiprofiles, and a line parallel to the model axis located at $r=(A_n/\pi)^{1/2}$ is defined (Fig. 5).

2) The centroid of this area, $\bar{y}$, about the model axis is found.

3) Assuming the the pre- and post-erosion nose tips are axisymmetric, the volume removed is that region swept out by rotating this area 360° about the model axis and is given by a theorem of Pappus[19] as

$$V_r = 2\pi\bar{y}A_p \tag{11}$$

4) Two such volumes are found for each laser photograph.

5) These values of volume removed are converted to mass removed

$$m_r = \rho_n V_r \tag{12}$$

6) An adjustment to m_r is made to account for the differences in the profile and the true surface contour. That is, "valleys" in the true contours may be obscured from view by adjacent "peaks" with the result being a larger eroded mass than predicted by the profile calculations.

7) Finally, the mass removed at each laser station m_n is taken to be the average value from all good quality photographs at that location.

The correction for the hidden surface contour bias was determined from a series of laboratory experiments. These experiments consisted of removing mass from a static nose tip to approximate in-flight erosion damage, determining the mass of material removed by weighing the undamaged and damaged specimen, taking static laser photographs of the damaged model simulating an actual range shot, determining mass removed from these photographs as if they were in-flight

Fig. 4 Sequence of in-flight front-lighted laser photographs.

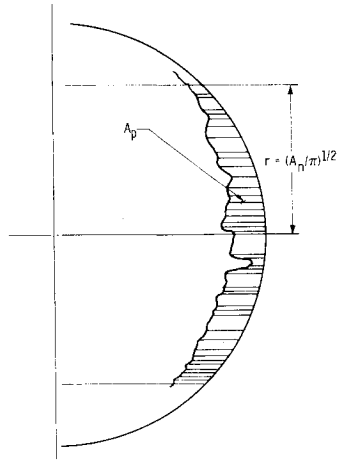

Fig. 5 Typical model profile.

photographs, and, finally, comparing the mass removed as determined from the photographs with the directly measured value. Values of this bias correction typically range from 5 to 15% of the eroded mass.

Data Uncertainty Analysis

The mass removal ratio is given by

$$G = m_n/m_s \tag{13}$$

Since m_n and m_s are independent variables having standard deviations of σ_{m_n} and σ_{m_s}, respectively, the standard deviation of G may be expressed[20] as

$$\sigma_G = \left[\left(\frac{\partial G}{\partial m_n}\right)^2_{m_s}\sigma^2_{m_n} + \left(\frac{\partial G}{\partial m_s}\right)^2_{m_n}\sigma^2_{m_s}\right]^{1/2} \tag{14}$$

where

$$\left(\frac{\partial G}{\partial m_n}\right)_{m_s} = \frac{1}{m_s} \tag{15}$$

and

$$\left(\frac{\partial G}{\partial m_s}\right)_{m_n} = -\frac{m_n}{m_s^2} \tag{16}$$

Finally

$$\sigma_G = \left[\frac{(m_s^2 \sigma_{m_n}^2 + m_n^2 \sigma_{m_s}^2)}{m_s^4} \right]^{1/2} \quad (17)$$

It is assumed that the errors contributing to the uncertainties in m_n and m_s are all normally distributed with zero mean. The "one-sigma" uncertainty bar is then $\pm\sigma_G$, meaning that for a large number of repeat shots, 68.26% deviate less than σ_G from the given value of G.

The primary uncertainties associated with determining the mass of snow impacted are taken to be the error in estimating the mass in the reference area, the error is assuming that the mass in the reference area is uniformly distributed, and the uncertainty involved in measuring only a portion of the snowfields.

The primary uncertainties associated with determining the mass of nose material removed are taken to be the profile measurement error, the eroded volume error, and the uncertainty in the hidden surface contour bias correction. Because of film response characteristics, motion blur, and finite optical resolution, the true and apparent profiles may be different. The best statistical approximation to the true profile is obtained and the associated uncertainty assessed. The resulting standard deviation is typically ± 1.5 mils.

These uncertainty components are evaluated from test data and snowfield calibration experiments. Total estimated "one-sigma" uncertainties in mass removal ratio after encountering 440 ft of snow environment are typically ± 15 to 25%.

Results

Figure 6 is an in-flight photograph of a model inside a snowfield at an encounter velocity of 8,000 fps. The striped background card permits visualization of some of the more prominent flow characteristics without sacrifice of surface detail resolution. The ejecta from the nose tip can be seen interacting without the model bow shock, and, in fact, a number of the particles are seen to be outside of the bow shock.

In Fig. 7 an in-flight laser photograph of a model nose tip is blown up to illustrate the pre- and post-erosion profiles. Figure 8 shows three frames from a sequence of in-flight, back-lighted photographs of the model taken during snowfield encounter. The photographs were taken with a Beckman and Whitley high-speed framing camera (Model No. 192) at a framing rate of 514,000 frames/sec. Individual snowflakes and debris clouds can be traced frame to frame.

A conventional, open-shutter, front-lighted, photograph of model-snowfield encounter is presented in Fig. 9. The snowflakes are double exposed by the strobe light and subsequent illumination from the nose tip. The luminous nose tip can be seen entering the field from the left with snowfield encounter resulting in a brilliant flash of light. Traces of what are apparently debris particles emanate from this flash. In addition, traces of debris particles that apparently originated at the previous snowfield encounter are observed entering the field of view from the left, well outside of the region swept out by the model.

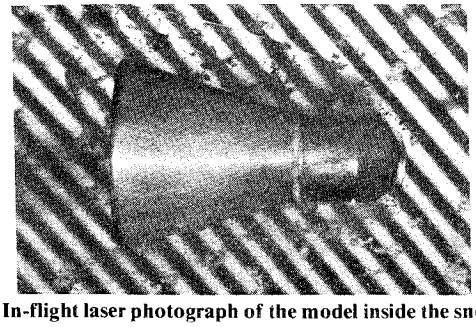

Fig. 6 In-flight laser photograph of the model inside the snowfield.

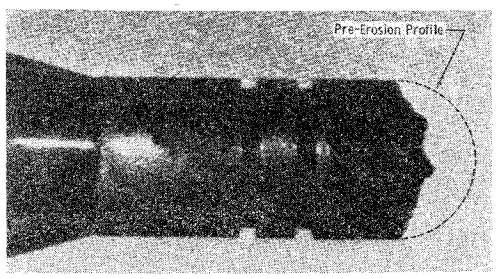

Fig. 7 Blow-up of an in-flight laser photograph.

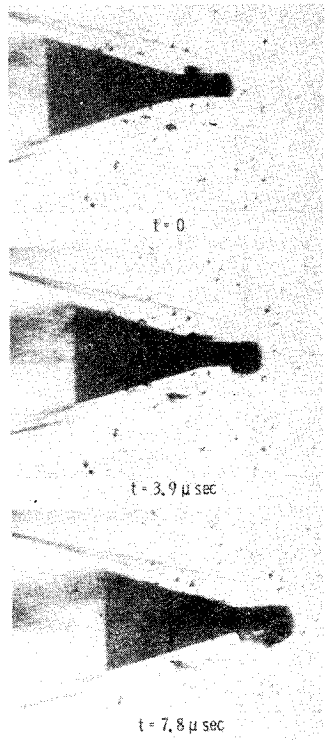

Fig. 8 Sequence of in-flight, back-lighted photographs of model-snowfield encounter.

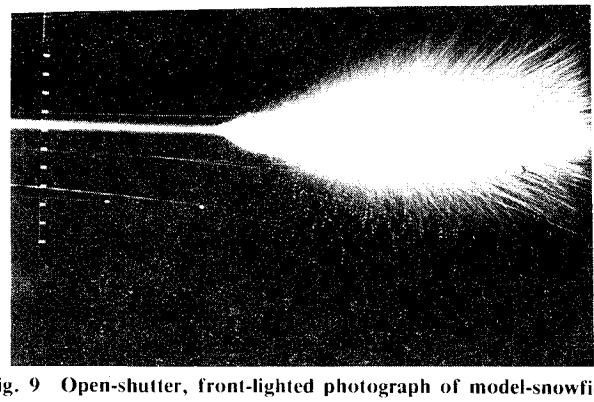

Fig. 9 Open-shutter, front-lighted photograph of model-snowfield encounter.

Summary

The unique snow erosion test capability described in this paper has been applied to test conditions for which erosion is the dominant mechanism as well as conditions for which significant ablation-erosion coupling is present. To date, 175 snow erosion tests have been conducted in Range G. These tests have been characterized by encounter velocities from 8,000 to 19,000 fps, model stagnation pressures from 20 to 200 atm, and snowfield concentrations down to 0.05 gm/m^3. These test conditions span the flight regimes of interest.

Acknowledgment

The research reported herein was done by the Arnold Engineering Development Center (AEDC), Air Force Systems Command (AFSC). The results were obtained by ARO, Inc., contract operator of AEDC. Further reproduction is authorized to satisfy needs of the U. S. Government.

References

[1]Norfleet, G. D., Hendrix, R. E., Raper, R. M., and Callens, E. E., Jr., "Development of an Aeroballistic Range Capability for Testing Re-Entry Materials," *Journal of Spacecraft and Rockets*, Vol. 12, May 1975, pp. 302-307.

[2]Nakaya, U., *Snow Crystals*, Harvard University Press, Cambridge, Mass., 1954.

[3]Mason, B. J., *The Physics of Clouds*, Clarendon Press, Oxford, 1971.

[4]Fletcher, N. H., *The Physics of Rain Clouds*, Cambridge University Press, New York, 1972.

[5]Byers, H. R., *Elements of Cloud Physics*, The University of Chicago Press, Chicago, 1965.

[6]Dufour, L. and Defay, R., *Thermodynamics of Clouds*, Academic Press, New York, 1963.

[7]Fleagle, R. G and Businger, J. A., *An Introduction to Atmospheric Physics*, Academic Press, New York, 1963.

[8]Clemens, P. L., "The von Karman Gas Dynamics Facility 1000-Ft Hypervelocity Range-Description, Capabilities and Early Test Results," Arnold Engineering Development Center, Arnold, AFB, Tenn., TR-66-197 (AD801906), Nov. 1966.

[9]Dugger, P. H. and Hill, J. W., "Laser Photographic Techiniques for Direct Photography in an Aeroballistic Range," Arnold Enginering Development Center, Arnold AFB, Tenn., TR-68-225 (AD683259), Feb. 1969.

[10]Dugger, P.H. and Hill, J.W., "A Laser Photographic System for Aeroballistic Range Photography," *ICIASF '68 Record*, May 1969, pp. 160-167.

[11]Dugger, P. H., et al., "Laser High-Speed Photography for Accurate Measurements of the Contours of Models in Hypervelocity Flight within an Aeroballistic Range," *Proceedings of the Electro-Optical Systems Design Conference*, New York, Sept. 1970, pp. 373-386.

[12]Dugger, P. H. and Hill, J. W., "A New Dimension in Front-Light Laser Photography," *AIAA Journal*, Vol. 10, Nov. 1972, pp. 1544-1546.

[13]Hill, J. W., "A Large Viewfield Laser Photographic System for In-Flight Model Contour Measurements in an Aeroballistic Range," *Proceedings of the 18th National Aerospace Instrumentation Symposium*, May 1972, Miami, Fla., pp. 17-22.

[14]Hendrix, R. E. and Dugger, P. H., "Instrumentation for an Aeroballistic Range Test Facility," *ICIASF '73 Record*, Sept. 1973, pp. 45-50.

[15]Hendrix, R. E. and Dugger, P. H., "Photographic Instrumentation in Hyperballistics Range (G) of the von Karman Gas Dynamics Facility," *Photographic Applications in Science, Technology and Medicine*, Sept. 1973, pp. 22-30.

[16]Dugger, P. H., et al., "A High-Speed Photographic Pyrometer," *Proceedings of Electro-Optics '71 East Conference*, New York, Sept. 1971, pp. 228-233.

[17]Dugger, P. H., et al., "Photographic Pyrometry in an Aeroballistic Range," *Proceedings of the SPIE 16th Annual Technical Meeting*, San Francisco, Calif., Oct. 1972, pp. 17-25.

[18]Dugger, P. H., "Aeroballistic Range Instrumentation Development," Arnold Engineering Development Center, Arnold AFB, Tenn., TR-76-146, Sept. 1976.

[19]Thomas, G. B., Jr., *Calculus and Analytic Geometry*, Addison-Wesley, Reading, Mass. 1958.

[20]Beers, Y., *Introduction to the Theory of Error*, Addison-Wesley, Reading, Mass. 1962.